A new SSI algorithm for LPTV systems: application to a hinged-bladed helicopter

Ahmed Jhinaoui, Laurent Mevel, Joseph Morlier

A new SSI algorithm for LPTV systems: Application to a hinged-bladed helicopter

Ahmed Jhinaoui [a], Laurent Mevel [a,*], Joseph Morlier [b]

[a] Inria, Centre Rennes - Bretagne Atlantique, 35042 Rennes, France
[b] Université de Toulouse, ICA/ISAE, 10 Av. Edouard Belin, Toulouse, France

ARTICLE INFO

Keywords:
Helicopter dynamics
Anisotropic rotor
Linear periodically time-varying (LPTV) systems
Linear time-periodic (LTP)
Floquet analysis
Subspace identification

ABSTRACT

Many systems such as turbo-generators, wind turbines and helicopters show intrinsic time-periodic behaviors. Usually, these structures are considered to be faithfully modeled as linear time-invariant (LTI). In some cases where the rotor is anisotropic, this modeling does not hold and the equations of motion lead necessarily to a linear periodically time-varying (referred to as LPTV in the control and digital signal field or LTP in the mechanical and nonlinear dynamics world) model. Classical modal analysis methodologies based on the classical time-invariant eigenstructure (frequencies and damping ratios) of the system no more apply. This is the case in particular for subspace methods. For such time-periodic systems, the modal analysis can be described by characteristic exponents called Floquet multipliers. The aim of this paper is to suggest a new subspace-based algorithm that is able to extract these multipliers and the corresponding frequencies and damping ratios. The algorithm is then tested on a numerical model of a hinged-bladed helicopter on the ground.

1. Introduction

Most existing identification techniques in mechanical and civil engineering work under the assumption that the underlying system can be modeled by a linear time-invariant (LTI) model. Unfortunately, structures that exhibit intrinsically time-varying behaviors are increasingly used in industry. For accurate analysis of such structures, that assumption is not satisfied. The time-varying aspect must be taken into account for a whole and reliable description of the system dynamics.

The extension of the well-known identification techniques to the linear time-varying (LTV) systems is an ongoing active topic of research. A wide range of methods have been suggested in the literature. Among them, one can cite the frozen-time approach introduced first in [1,2] which deals with the identification of slowly time-varying systems (the frozen-time approach consists in modeling the slowly time varying system as a sequence of LTI systems, called frozen-time systems). Recursive algorithms such as recursive least squares (RLS), recursive instrumental variable and recursive predictive error [3,4] have also been widely investigated. For the class of rapidly time-varying systems, the functional expansion techniques have been suggested in manifold works [5–8].

In [9–12], efforts have been undertaken to extend the subspace identification approach [13] to the LTV case by introducing the idea of repeated experiments. As pointed in [14], most subspace-based results developed thus far, even if significant, give state space realizations that are topologically equivalent from an input and output standpoint, but are not

* Corresponding author. Tel.: +33 2 99 84 73 25; fax: +33 2 99 84 71 71.
E-mail address: laurent.mevel@inria.fr (L. Mevel).

defined in the same coordinate system. In other words, between two different instants the identified realizations will be expressed in two different bases.

Mechanical engineers are rather interested in identifying system eigenvalues and eigenvectors (which give modal frequencies, damping ratios and mode shapes) for vibration and stability analysis sake. Unfortunately and due to the lack of a consistent theoretical background, the modal analysis of time-varying systems is not well defined and is still handled case by case. The eigenvalues, for example, of each of the identified state space matrices, using the subspace framework, do not determine the stability of the global system as illustrated by example in [15] and as in [11] where the concept of pseudo-eigenvalues is preferred to eigenvalues.

The scope herein is limited to a sub-class of LTV which is the linear periodically time-varying (LPTV or LTP) class. Time-periodic systems are considered to be a bridge between the time-invariant case and the time varying one, and their theory is well established. In fact, the modal analysis of ordinary differential equations (ODE) with periodic coefficients, known as Mathieu's equation [16], was handled using the Floquet theory [17], in many works [18–22]. This theory derives some characteristic multipliers, called the Floquet multipliers (or Lyapunov–Floquet multipliers), that stand for the classical eigenvalues. When not canceled by system's zeros (anti-resonance, for example), these multipliers entirely describe the dynamics of a time-periodic system and predict its stability margins. In the time domain, the extraction of those multipliers has so far lied to the computation of the fundamental solution matrix (FSM) [23] from the integration of the system equations. Then, a so-called monodromy matrix, whose eigenvalues derive the Floquet multipliers, is deduced. The integration of periodic ODE is immensely costly and cumbersome. In [24,25] for example, a technique employing expansion in Chebyshev polynomials is used in order to symbolically approximate the FSM and alleviate the computational burden of the exact solution. This symbolic approximate solution is still computationally costly.

Despite these significant analytic results which assume that the differential equation is known, scope on the identification of the Floquet multipliers and the corresponding mode shapes from output-only data remains limited. Allen and coworkers are the first who have taken steps in this direction in [26–28]. They used, for the purpose, the harmonic transfer function concept by Wereley and Hall [29], which is an extension of the concept of transfer function to LPTV systems.

In this paper, we suggest a new time-domain subspace-based algorithm which is able to extract the Floquet multipliers and mode shapes of an LPTV systems from output-only data. The originality is to build a subspace matrix from the covariances of two lagged subsequences of the output data that have same dynamics, in such a way that the monodromy matrix is a least square approximation of an equation involving two block rows of the said subspace matrix.

The paper is organized as follows: in Section 2, a classical output-only stochastic subspace identification (SSI) algorithm for LTI systems is presented. Then, Section 3 is devoted to the extension of this algorithm to periodic cases. The new algorithm is designed so that it extracts the Floquet multipliers and mode shapes of an LPTV system. Finally in Section 4, the algorithm has been tested on a numerical simulation of a helicopter with a hinged-blades rotor on the ground.

2. A classical output-only subspace identification algorithm

In this section, a typical output-only stochastic subspace (SSI) algorithm, based on covariance-driven data, is presented [30]. Let the LTI continuous-time state space model of a given system be

$$\begin{cases} \dot{z}(t) = A\, z(t) + v(t) \\ y(t) = C\, z(t) + w(t) \end{cases} \tag{1}$$

where $z \in \mathbb{R}^n$ is the state vector, $y \in \mathbb{R}^r$ the output vector or the observation, $A \in \mathbb{R}^{n\times n}$ the state matrix and $C \in \mathbb{R}^{r\times n}$ the observation matrix. The vectors v and w are uncorrelated noises assumed to be white Gaussian such that their means and covariances are defined as follows:

$$\mathbf{E}(v(s)) = 0, \quad \mathbf{E}(v(s)v^T(s')) = Q_v \cdot \delta(s-s')$$

$$\mathbf{E}(w(s)) = 0, \quad \mathbf{E}(w(s)w^T(s')) = Q_w \cdot \delta(s-s')$$

where $\mathbf{E}$ is the expectation operator and δ is the Dirac function. Consider a sampling period τ and denote by

$$F = e^{A\tau}, \quad z_k = z(k\tau), \quad y_k = y(k\tau),$$

$$w_k = w(k\tau), \quad \tilde{v}_k = \int_{k\tau}^{(k+1)\tau} e^{A((k+1)\tau - s)} v(s)\, ds$$

The discrete-time form of (1) is written as [31]

$$\begin{cases} z_{k+1} = Fz_k + \tilde{v}_k \\ y_k = Cz_k + w_k \end{cases} \tag{2}$$

As shown in [31], the resulting sequence $\{\tilde{v}_k\}$ is an uncorrelated white noise. Its mean and covariance are respectively

$$\mathbf{E}(\tilde{v}_k) = \mathbf{E}\left(\int_{k\tau}^{(k+1)\tau} e^{A((k+1)\tau-s)} v(s)\, ds\right) = \int_{k\tau}^{(k+1)\tau} e^{A((k+1)\tau-s)} \underbrace{\mathbf{E}(v(s))}_{0} ds = 0 \tag{3}$$

and

$$\begin{aligned}
\mathbf{E}(\tilde{v}_k \tilde{v}_k^T) &= \mathbf{E}\left(\int_{k\tau}^{(k+1)\tau}\int_{k\tau}^{(k+1)\tau} e^{A((k+1)\tau-s)} v(s) v^T(s') e^{A^T((k+1)\tau-s')}\, ds\, ds'\right) \\
&= \int_{k\tau}^{(k+1)\tau}\int_{k\tau}^{(k+1)\tau} e^{A((k+1)\tau-s)} \underbrace{\mathbf{E}(v(s)v^T(s'))}_{Q_v\cdot\delta(s-s')} e^{A^T((k+1)\tau-s')}\, ds\, ds' \\
&= \int_{k\tau}^{(k+1)\tau} e^{A((k+1)\tau-s)} \underbrace{\mathbf{E}(v(s)v^T(s))}_{Q_v} e^{A^T((k+1)\tau-s)}\, ds = \int_0^{\tau} e^{A((k+1)\tau-s)} \cdot Q_v \cdot e^{A^T((k+1)\tau-s)}\, ds
\end{aligned} \tag{4}$$

Let λ and ϕ_λ be respectively the eigenvalues and the eigenvectors of system (2):

$$\det(F-\lambda I) = 0, \quad F\phi_\lambda = \lambda\phi_\lambda \tag{5}$$

Denote $\psi_\lambda = C\phi_\lambda$ the observed eigenvectors, also called mode shape. The objective of identification is to extract the eigenstructure (λ, ψ_λ) using the available output data from the sensors. The steps of the SSI algorithm are given hereafter.

For chosen parameters p and q such that $\min\{pr, qr\} \geq n$, the covariance-driven Hankel matrix below $\mathcal{H}_{p,q} \in \mathbb{R}^{(p+1)r\times qr}$ is built:

$$\mathcal{H}_{p,q} = \begin{bmatrix} R_1 & R_2 & \cdots & R_q \\ R_2 & R_3 & \cdots & R_{q+1} \\ \vdots & \vdots & \vdots & \vdots \\ R_{p+1} & R_{p+2} & \cdots & R_{p+q} \end{bmatrix} \tag{6}$$

with $R_i = \mathbf{E}(y_k y_{k-i}^T)$ the covariances of the output data. If N is the number of output measurements that are available ($N \gg 1$), the R_i's can be estimated by

$$\hat{R}_i = \frac{1}{N}\sum_{k=i+1}^{N} y_k y_{k-i}^T$$

In practice, the parameters p and q are chosen sufficiently large such that the order of the Hankel matrix is equal to the system order n. Also, a classical choice for covariance driven subspace approaches is to take $q = p+1$ to ensure that the subspace matrix is square. These considerations are extensively treated in [32–34].

An estimate of the Hankel matrix can be written as

$$\hat{\mathcal{H}}_{p,q} = \frac{1}{N}\sum_{k=q+1}^{N-p} \mathcal{Y}_k^+ \mathcal{Y}_k^{-T} \tag{7}$$

where

$$\mathcal{Y}_k^+ = [y_k^T \ \cdots \ y_{k+p}^T]^T, \quad \mathcal{Y}_k^- = [y_{k-1}^T \ \cdots \ y_{k-q}^T]^T \tag{8}$$

Let $G = \mathbf{E}(z_k y_k^T)$ be the correlation between the state and the observation, $\mathcal{O}_p = [C^T, (CF)]^T, \ldots, [(CF^p)^T]^T$ and $\mathcal{C}_q = [FG, F^2G, \ldots, F^qG]$ the p-th order observability matrix and the q-th order (shifted) controllability matrix respectively. The computation of the R_i's leads to the decomposition [30]:

$$\mathcal{H}_{p,q} = \mathcal{O}_p \mathcal{C}_q \tag{9}$$

Therefore, an estimate $\hat{\mathcal{O}}_p$ of the observability matrix can be obtained via a Singular Value Decomposition (SVD) of the Hankel matrix $\hat{\mathcal{H}}_{p,q}$ and its truncation at the desired model order n [35]. This estimate is obtained up to a non-singular matrix:

$$\hat{\mathcal{H}}_{p,q} = U\Delta V^T = [U_1 \ U_2]\begin{bmatrix}\Delta_1 & 0 \\ 0 & \Delta_2\end{bmatrix}\begin{bmatrix}V_1^T \\ V_2^T\end{bmatrix} \quad U \in \mathbb{R}^{(p+1)r\times(p+1)r}, \quad \Delta \in \mathbb{R}^{(p+1)r\times qr}, \text{ and } V \in \mathbb{R}^{qr\times qr} \tag{10}$$

$$\hat{\mathcal{O}}_p = U_1 \Delta_1^{1/2} \tag{11}$$

where $\Delta_1 \in \mathbb{R}^{n\times n}$ contains the n first singular values and $U_1 \in \mathbb{R}^{(p+1)r\times n}$ the n first columns of $U \in \mathbb{R}^{(p+1)r\times(p+1)r}$. Since only the left part of the singular value decomposition is needed to retrieve an estimate of the observability matrix, an economic (so-called *thin*) SVD, which computes only that left part, can be used.

An estimate $\hat{C}$ of the observation matrix is extracted from the first r rows of the observability matrix $\hat{\mathcal{O}}_p$. The estimate $\hat{F}$ of the state transition matrix is obtained from a least square approximation of [30]:

$$\mathcal{O}_p^{\uparrow} F = \mathcal{O}_p^{\downarrow} \tag{12}$$

where $\mathcal{O}_p^{\uparrow}$ and $\mathcal{O}_p^{\downarrow}$ are defined as

$$\mathcal{O}_p^{\uparrow} = \begin{bmatrix} C \\ CF \\ \vdots \\ CF^{p-1} \end{bmatrix}, \quad \mathcal{O}_p^{\downarrow} = \begin{bmatrix} CF \\ CF^2 \\ \vdots \\ CF^{p} \end{bmatrix} \tag{13}$$

and can be respectively estimated as the first pr rows and the last pr rows of the estimated observability matrix $\hat{\mathcal{O}}_p$. Once the state transition matrix F and the observation matrix C are estimated, the system eigenstructure can be easily retrieved.

3. Subspace identification for LPTV systems

In this section, the classical SSI algorithm presented in Section 2 is extended to the case of linear periodically time-varying systems. Since in real applications, the time-invariant modal description may yield misleading results for such systems [22,26], we introduce a general description based on the Floquet theory. The essential elements of this theory are recalled, then the steps of the new algorithm are detailed.

3.1. On Floquet theory

The Floquet theory is a mathematical theory of ordinary differential equations (ODE) with time-periodic coefficients. Introduced by Floquet in [17], it is the first complete theory for the class of periodically time-varying systems. Some of its essential elements, that are related to the study hereafter, are briefly reviewed. More details can be found in [36].

Let us consider the periodic differential system:

$$\dot{x}(t) = A(t)x(t) \tag{14}$$

where $x \in \mathbb{R}^n$ is the state vector. The state transition matrix $A(t) \in \mathbb{R}^{n\times n}$ is continuous in time (or at least, piecewise continuous) and periodic, of period $T > 0$. If an initial condition $x(t_0) = x_0$ is fixed, a solution of (14) is guaranteed to exist.

Let $\Phi(t)$ be the matrix whose n columns are n linearly independent solutions of (14), $\Phi(t)$ is known as the *fundamental transition matrix* (FTM). It has the properties:

$$\dot{\Phi}(t) = A(t)\Phi(t), \quad \Phi(t+T) = \Phi(t)\Phi(T), \quad \forall t \tag{15}$$

Let Q be the value of the fundamental matrix at $t=T$ (Q is called the *monodromy matrix*. It can be complex, even if the dynamical matrix $A(t)$ is real) and the matrix R such that

$$Q = \Phi(T), \quad R = \frac{1}{T}\log(Q) \tag{16}$$

The eigenvalues of R are called the Floquet exponents. They wholly describe the system (14) and replace the classical frequencies and damping ratios in the periodic case. Since R gives the information about the system dynamics [18], the goal hereafter is to identify this matrix (or its discretized form).

Make the change of variable $x(t) = \Phi(t)e^{-Rt}z(t)$. The theory insures that

$$\dot{z}(t) = Rz(t) \tag{17}$$

This transform is called the Lyapunov–Floquet transform (or Floquet transform). It gives an underlying *autonomous system* (a system with a constant state transition matrix with respect to time) that is equivalent to the initial periodic system (14).

Consider the complete system with the observation equation:

$$\begin{cases} \dot{x}(t) = A(t)x(t) + v(t) \\ y(t) = C(t)x(t) + w(t) \end{cases} \tag{18}$$

Both of the state transition matrix $A \in \mathbb{R}^{n\times n}$ and the observation matrix $C \in \mathbb{R}^{r\times n}$ are real, piecewise continuous and periodic of period T. The vectors v and w are unmeasured uncorrelated noises assumed to be white Gaussian. By Lyapunov–Floquet transformation, Eq. (18) is transformed into

$$\begin{cases} \dot{z}(t) = Rz(t) + (L(t))^{-1}v(t) \\ y(t) = \tilde{C}(t)z(t) + w(t) \end{cases} \tag{19}$$

where $L(t) = \Phi(t)e^{-Rt}$ and $\tilde{C}(t) = C(t)L(t)$. Since L is periodic, the new observation matrix $\tilde{C}(t)$ is periodic.

This transformation makes the modal analysis straightforward and comprehensive for periodic systems [37]: the modal frequencies are derived from the eigenvalues of R (called *Floquet exponents*) and the mode shapes are the product of the eigenvectors by the periodic matrix $\tilde{C}$ t C t L t . Let μ ρ $i\omega_p$ be a Floquet exponent (i $\sqrt{}$ 1). Then, as in the

y_j	y_{j+Td}	y_{j+2Td}	y_{j+3Td}	$\cdots$
z_j	z_{j+Td}	z_{j+2Td}	z_{j+3Td}	$\cdots$

Fig. 1. The j-th time-invariant subsequence.

time-invariant case the damping ratio and the modal frequency are defined as

$$\xi = \frac{-\rho}{|\omega_p|\sqrt{1+\rho^2/\omega_p^2}}, \quad f_p = \frac{|\omega_p|\sqrt{1+\rho^2/\omega_p^2}}{2\pi} \tag{20}$$

Let τ be a sampling period. The discretization of Eq. (19) yields the following:

$$\begin{cases} z_{k+1} = Fz_k + \tilde{v}_k \\ y_k = \tilde{C}_k z_k + w_k \end{cases} \tag{21}$$

where $z_k = z(k\tau)$, $y_k = y(k\tau)$, $F = e^{R\tau}$, $\tilde{C}_k = \tilde{C}(k\tau)$, $w_k = w(k\tau)$ and $\tilde{v}_k = \int_{k\tau}^{(k+1)\tau} e^{R((k+1)\tau - s)}(L(s))^{-1} v(s)\, ds$. Assume that the sampling period τ is a divisor of the system period T, then the obtained discrete-time system is periodic of period $T_d = T/\tau$.

The results (3) and (4) reported in [31] for the discrete-time noise in the time-invariant case can be readily extended to this periodic case:

$$\mathbf{E}(\tilde{v}_k) = \mathbf{E}\left(\int_{k\tau}^{(k+1)\tau} e^{R((k+1)\tau - s)}(L(s))^{-1} v(s)\, ds \right) = \int_{k\tau}^{(k+1)\tau} e^{R((k+1)\tau - s)}(L(s))^{-1} \underbrace{\mathbf{E}(v(s))}_{0} ds = 0 \tag{22}$$

and similarly

$$\mathbf{E}(\tilde{v}_k \tilde{v}_k^T) = \int_{k\tau}^{(k+1)\tau} e^{R((k+1)\tau - s)} L^{-1}(s) \cdot Q_v \cdot L^{-T}(s) e^{R^T((k+1)\tau - s)}\, ds \tag{23}$$

Consider the covariance of the obtained noise $\mathbf{E}(\tilde{v}_{k+T_d} \tilde{v}_{k+T_d}^T)$ at sample $(k+T_d)$ corresponding to the continuous time $(k\tau+T)$, and the variable change $\xi = s - T$:

$$\begin{aligned} \mathbf{E}(\tilde{v}_{k+T_d} \tilde{v}_{k+T_d}^T) &= \int_{k\tau+T}^{(k+1)\tau+T} e^{R((k+1)\tau+T-s)} L^{-1}(s) \cdot Q_v \cdot L^{-T}(s) e^{R^T((k+1)\tau+T-s)}\, ds \\ &= \int_{k\tau}^{(k+1)\tau} e^{R((k+1)\tau-\xi)} L^{-1}(\xi+T) \cdot Q_v \cdot L^{-T}(\xi+T) e^{R^T((k+1)\tau-\xi)}\, d\xi \\ &= \int_{k\tau}^{(k+1)\tau} e^{R((k+1)\tau-\xi)} L^{-1}(\xi) \cdot Q_v \cdot L^{-T}(\xi) e^{R^T((k+1)\tau-\xi)}\, d\xi = \mathbf{E}(\tilde{v}_k \tilde{v}_k^T) \end{aligned}$$

The purpose of the identification algorithm below is to extract the discrete-time Floquet exponents (namely, the eigenvalues of F) and the corresponding frequencies and damping ratios. If λ is an eigenvalue of F, then it is related to the continuous-time Floquet exponent μ by $\lambda = e^{\mu\tau}$, and the modal frequency and the damping ratio are derived from Eq. (20).

The focus of this paper is the poles of the system and the corresponding frequencies and damping ratios. Nonetheless, the extraction of the mode shapes is straightforward. The discrete-time and continuous-time transition matrices F and R have the same eigenvectors. Denote ϕ_{λ_i} the eigenvector corresponding to the i-th eigenvalue λ_i, hence the i-th mode shape at instant k is equal to $\psi_{k,i} = \tilde{C}_k \phi_{\lambda_i}$.

3.2. Identification algorithm

The subsequences $(z_{j+iT_d})_{i \in \mathbb{N}}$ and $(y_{j+iT_d})_{i \in \mathbb{N}}$ have the same dynamics for all j. A total of T_d different subsequences exists [38]. One of these subsequences (denoted the j-th subsequence in the following) is shown in Fig. 1.

Let p and q be two parameters such that $\min\{pr, qr\} \geq n$. A Hankel matrix, built on the j-th index, is defined as

$$\hat{\mathcal{H}}_{p,q}^{(j)} = \frac{1}{N_T} \sum_{i=0}^{N_T-1} \mathcal{Y}_{j+iT_d}^{+} \mathcal{Y}_{j+iT_d}^{-T} \tag{24}$$

where N_T is the number of the available rotor revolutions (number of periods). The parameters p and q are chosen as in the time-invariant case. Notice that more than one subsequence is used, i.e. for one choice of the index j, all points between $j-q$ and $j+p$ are used at every period, to compute the Hankel matrix $\hat{\mathcal{H}}_{p,q}^{(j)}$ resulting from the summation of the products $\mathcal{Y}_{j+iT_d}^{+} \mathcal{Y}_{j+iT_d}^{-T}$. Still, decimating the summation at every period will yield to Proposition 3.1.

Proposition 3.1. *When N_T goes to infinity, the Hankel matrix can be factorized as follows*:

$$\mathcal{H}_{p,q}^{(j)} = \mathcal{O}_p^{(j)} \mathcal{C}_q^{(j)} \tag{25}$$

where the observability and the controllability matrices are defined as

$$\mathcal{O}_p^{(j)} = \begin{bmatrix} \tilde{C}_j \\ \tilde{C}_{j+1}F \\ \vdots \\ \tilde{C}_{j+p}F^{j+p} \end{bmatrix} \tag{26}$$

$$\mathcal{C}_q^{(j)} = [FG^{(j-1)} \ \cdots \ F^q G^{(j-q)}] \tag{27}$$

where $G^{(k)}$ *is the state-output cross correlation of the k-th invariant subsequence. It can be estimated by* $\hat{G}^{(k)} = (1/N_T)\sum_{i=0}^{N_T-1} z_{k+iT_d} y_{k+iT_d}^T$.

Proof. See Appendix A for the proof.

In [39,40], the authors proposed a subspace-based algorithm for the extraction of the Floquet multipliers from the computation of two successive Hankel matrices $\mathcal{H}_{p,q}^{(j)}$ and $\mathcal{H}_{p,q}^{(j+1)}$, then a resolution of a least squares equation. This algorithm estimates the matrix F up to two different time-varying transforms $\hat{T}^{(j)}$ and $\hat{T}^{(j+1)}$, such that the output of the algorithm is related to the desired estimate as $\hat{T}^{(j+1)^{-1}}\hat{F}\hat{T}^{(j)}$. In order to solve this problem some approximation has been made as in [10]. This approximation may hold only for very low rotation speeds. In the current paper, the proposed algorithm solves the problem without any approximation, and is then applicable for rotating systems with high and low rotation speeds. The idea is to build the Hankel matrix denoted $\hat{\mathcal{H}}_{p,q}^{(j+)}$, such that the future data are shifted from the past data by a period T_d:

$$\hat{\mathcal{H}}_{p,q}^{(j+)} = \frac{1}{N_T}\sum_{i=0}^{N_T-1} \mathcal{Y}_{j+(i+1)T_d}^{+} \mathcal{Y}_{j+iT_d}^{-T} \tag{28}$$

Since $\tilde{C}_k$ and $G^{(k)}$ are periodic for all k, we get the following limit factorization:

$$\mathcal{H}_{p,q}^{(j+)} = \mathcal{O}_p^{(j+T_d)} F^{T_d} \mathcal{C}_q^{(j+T_d)} = \mathcal{O}_p^{(j)} F^{T_d} \mathcal{C}_q^{(j)} \tag{29}$$

Consider the total Hankel matrix:

$$\mathcal{H}_{p,q} = \begin{bmatrix} \mathcal{H}_{p,q}^{(j)} \\ \mathcal{H}_{p,q}^{(j+)} \end{bmatrix} = \begin{bmatrix} \mathcal{O}_p^{(j)} \\ \mathcal{O}_p^{(j)} F^{T_d} \end{bmatrix} \mathcal{C}_q^{(j)} = \mathcal{O}_p \mathcal{C}_q^{(j)} \tag{30}$$

and

$$\hat{\mathcal{H}}_{p,q} = \begin{bmatrix} \hat{\mathcal{H}}_{p,q}^{(j)} \\ \hat{\mathcal{H}}_{p,q}^{(j+)} \end{bmatrix} \tag{31}$$

Obviously, the total observability matrix $\mathcal{O}_p$ depends on the sample index j. This dependency is dropped, for the sake of notation simplicity. An estimate $\hat{\mathcal{O}}_p$ of $\mathcal{O}_p$ can be obtained from a singular value decomposition of the total Hankel matrix estimate $\hat{\mathcal{H}}_{p,q}$. $\hat{\mathcal{O}}_p$ is obtained up to some non-singular matrix $\hat{T}$. Denote $\mathcal{O}_p^{\uparrow}$ the first $(p+1)$ block rows of $\mathcal{O}_p$ and $\mathcal{O}_p^{\downarrow}$ the last block rows. Define their estimates accordingly. The transition matrix F satisfies

$$\mathcal{O}_p^{\uparrow} F^{T_d} = \mathcal{O}_p^{\downarrow} \tag{32}$$

Then an estimate of the transition matrix F can be retrieved as

$$\hat{F} = ((\hat{\mathcal{O}}_p^{\uparrow})^{\dagger} \hat{\mathcal{O}}_p^{\downarrow})^{1/T_d} \tag{33}$$

Since we only have an estimate of the observability matrix $\mathcal{O}_p$ up to some transform $\hat{T}$, then the estimate of F is defined up to an invertible matrix $\hat{T}$. Notice that the basis $\hat{T}$ is a byproduct of the singular value decomposition procedure but has no impact on the eigenvalues of $\hat{F}$ since two estimates related by

$$\hat{F}_1 = \hat{T}^{-1}\hat{F}_2\hat{T} \tag{34}$$

are two representations of the same linear map (the transform matrix $\hat{T}$ is the same in the left and the right). Once the discrete-time Floquet exponents (the eigenvalues of $\hat{F}$) and the corresponding eigenvectors are identified, the modal frequencies, the damping ratios and the mode shapes can be deduced. Those quantities do not depend on $\hat{T}$. A summary of the identification steps is given in Algorithm 1.

Algorithm 1. Floquet exponents identification.

Require: $(N_T T_d + p + j)$ output data (y_k) are available.
1: Initialization: $\hat{\mathcal{H}}_{p,q}^{(j)} \leftarrow 0_{(p+1)r\times qr}$ and $\hat{\mathcal{H}}_{p,q}^{(j+)} \leftarrow 0_{(p+1)r\times qr}$. Take q and p such that $\min\{pr, qr\} \geq n$
2: **for** $i = 0 : (N_T - 1)$ **do**
3: $\hat{\mathcal{H}}_{p,q}^{(j)} \leftarrow \hat{\mathcal{H}}_{p,q}^{(j)} + \mathcal{Y}_{j+iT_d}^{+} \mathcal{Y}_{j+iT_d}^{-T}$ as in Eq. (24)
4: **end for**
5: **for** $i = 0 : (N_T - 1)$ **do**

6: $\hat{\mathcal{H}}_{p,q}^{(j+)} \leftarrow \hat{\mathcal{H}}_{p,q}^{(j+)} + \mathcal{Y}_{j+(i+1)T_d}^{+} \mathcal{Y}_{j+iT_d}^{-T}$ as in Eq. (28)
7: **end for**
8: $\hat{\mathcal{H}}_{p,q} \leftarrow \begin{bmatrix} \hat{\mathcal{H}}_{p,q}^{(j)} \\ \hat{\mathcal{H}}_{p,q}^{(j+)} \end{bmatrix}$
9: compute the SVD of $\hat{\mathcal{H}}_{p,q}$
10: retrieve $\hat{\mathcal{O}}_p$, $\hat{\mathcal{O}}_p^{\uparrow}$ and $\hat{\mathcal{O}}_p^{\downarrow}$
11: compute an estimate $\hat{F} \leftarrow ((\hat{\mathcal{O}}_p^{\uparrow})^{\dagger} \hat{\mathcal{O}}_p^{\downarrow})^{1/T_d}$
12: compute the Floquet exponents and the corresponding eigenvectors
13: deduce the frequencies, damping ratios and mode shapes
Ensure: the system modal frequencies, damping ratios and mode shapes

4. Application

4.1. Helicopter model

In this section, the suggested identification method is tested on a helicopter model. We give, first, some essential elements that allow to understand the dynamics of a helicopter on the ground and the instabilities that may occur, namely the ground resonance.

When the rotor of a helicopter is spinning, some angular phase shifts – known as leading and lagging angles – can be created on the blades by external disturbances. Basically, this may occur when a helicopter with a wheel-type landing gear touches the ground firmly on one corner, then this shock is transmitted to the blades in the form of out of phase angular motions. Those angular motions interact with the elastic parts of the fuselage (the landing gear, mainly) for certain values of rotor's angular velocity. The fuselage starts then to rock laterally. These lateral oscillations amplify the lead-lagging motions which also amplify the fuselage oscillations, and so on till the divergence and the destruction of the structure when a critical rotation velocity is reached.

The analysis given herein is based on the model in [41], but extending it to the case where dampers are present on the structure. The fuselage is considered to be a rigid body with mass M, attached to a flexible landing gear (LG) which is modeled by two springs K_x and K_y, and two viscous dampers C_x and C_y as illustrated in Fig. 2. For the sake of simplicity, the fuselage is considered to be symmetrical: namely the stiffnesses are equal to the same value, K_z, $K_x = K_y = K_z$ and idem for the viscous dampers $C_x = C_y = C_z$. The rotor spinning with a velocity Ω is articulated and the offset between the MR (main rotor) and each articulation is noted as a. For $k = 0, \ldots, N_b - 1$ (with N_b the number of blades), each blade is modeled by a concentrated mass m – considered constant here for the sake of simplicity – at a distance b of the articulation point and a torque stiffness and a viscous damping K_{ϕ_k} and C_{ϕ_k} are present in each articulation. The moment of inertia around each articulation point is I_z. The degrees of freedom are the lateral displacements of the fuselage x and y, and the out-of-phase angles (ϕ_k).

The equation of motion of the studied mechanical system is obtained by applying Lagrange equations to the kinetic, potential energy and dissipation function's expressions (respectively T, U and F) of the helicopter, given in Appendix B:

$$\frac{\delta}{\delta t}\left(\frac{\delta T}{\delta \dot{\xi}}\right) - \frac{\delta T}{\delta \xi} + \frac{\delta U}{\delta \xi} + \frac{\delta F}{\delta \dot{\xi}} = 0 \tag{35}$$

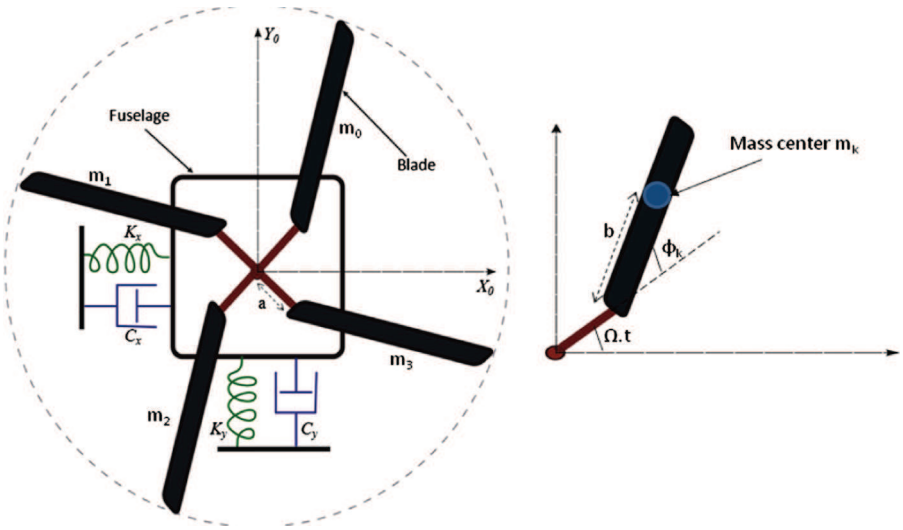

Fig. 2. Mechanical model of a 4 bladed helicopter: $N_b = 4$.

Table 1
Structural properties for hinged-blades helicopter with 4 blades [41].

Structural variable	Name	Value
Blade mass	m	31.9 kg
Fuselage mass	M	2902.9 kg
Blade stiffness	K_ϕ	1.0313×10^3 N/m
LG stiffness in the axis x	K_x	2.7275×10^4 N/m
LG stiffness in the axis y	K_y	2.7275×10^4 N/m
Blade damping coef.	C_ϕ	41.252 N s/m
LG damping in the axis x	C_x	1.091×10^3 N s/m
LG damping in the axis y	C_y	1.091×10^3 N s/m
Rotor eccentricity	a	0.2 m
Blade length	b	2.5 m
Blade inertial moment	I_z	259 kg m^2

Table 2
Classical and new algorithms results compared to true values for $\Omega = 3.5$ rad/s.

Mode	Classical SSI		New SSI		True values	
	Freq. (Hz)	D. ratio	Freq. (Hz)	D. ratio	Freq. (Hz)	D. ratio
1	**0.4769**	**0.1124**	**0.0853**	**0.3393**	**0.0850**	**0.3384**
2	**0.485**	**0.0526**	**0.0939**	**0.2948**	**0.0928**	**0.2936**
3	0.2263	0.0438	0.2277	0.0396	0.234	0.0316
4	0.2567	0.022	0.2589	0.0306	0.2597	0.0276
5	0.259	0.033	0.2607	0.0274	0.2604	0.0275
6	0.273	0.05	0.2744	0.0385	0.2751	0.0324

ξ is a dummy variable which is replaced by the system variables. Let q be the vector containing these variables $q = [x, y, \phi_0, \phi_1, \ldots, \phi_{N_b-1}]^T$. In our case, the behavior of the helicopter is described by the equation:

$$\mathcal{M}(t)\ddot{q} + \mathcal{C}(t)\dot{q} + \mathcal{K}(t)q = 0 \tag{36}$$

The matrices $\mathcal{M}$, $\mathcal{C}$ and $\mathcal{K}$ are respectively mass, stiffness and damping matrices. Their expressions are given in Appendix C. The system matrices are periodic with a period $T = 2\pi/\Omega$:

$$\mathcal{M}(t+T) = M(t), \quad \mathcal{C}(t+T) = \mathcal{C}(t), \quad \mathcal{K}(t+T) = \mathcal{K}(t), \quad \forall t \geq 0 \tag{37}$$

The model can be rewritten as in (18), taking the state variable $\mathcal{X}(t) = \begin{bmatrix} q(t) \\ \dot{q}(t) \end{bmatrix}$ and the state matrix $A(t) = \begin{bmatrix} 0 & \mathcal{I} \\ -\mathcal{M}^{-1}(t)\mathcal{K}(t) & -\mathcal{M}^{-1}(t)\mathcal{C}(t) \end{bmatrix}$ where $\mathcal{I}$ is the identity matrix.

4.2. Numerical simulation

Let us consider a helicopter with 4-bladed rotor, for this numerical application. And let the numerical values in Table 1 be the structural parameters of the considered helicopter. The numerical values are those of the model in [41], adding viscous dampers to it. In order to mimic the dynamics of a real helicopter, the values of the damping coefficients are taken such that $C_x = K_x/25$ and $C_\phi = K_\phi/25$ as in [42].

A standard white Gaussian signal with a unit standard deviation σ_v is generated for the state noise v. A white Gaussian noise w with a standard deviation σ_w is also generated such that the ratio $\sigma_v/\sigma_w = 10^3$. To simulate an anisotropy in the rotor, the stiffness of the fourth blade is taken such that $K_{\phi_3} = 0.75K_\phi$. We take the observation matrix $C = [0_{10\times 2}\ \mathcal{I}_{10\times 10}]$.

To simulate the data y_k, Eq. (14) is numerically integrated using the Runge–Kutta method.

4.3. Identification results

For $\Omega = 3.5$ rad/s, a first data set is generated over a number of rotor revolutions N_T=2000, with a discrete period T_d=100 (the sampling frequency is $F_s = T_d/T$). The order of the system is assumed to be known and is n=12. The suggested identification algorithm is applied to the data as explained herein before. The parameters p and q are chosen such that $q = p + 1 = 31$. The summary of the identified frequencies and damping ratios using the classical and the new SSI algorithms, as well as the true values, is given in Table 2. For each value of Ω, the new SSI is performed using N_T=2000 data samples where the classical algorithm uses N=200,000 samples. For the true modes, the monodromy matrix is computed from the Runge–Kutta numerical integration $Q = e^{\int_0^T A(t)\,dt}$. Then, the eigenvalues and the corresponding modal parameters (frequency and damping ratio) are deduced using (20).

Table 3
Variation of relative errors for new SSI with respect to sample length.

Mode	Frequency error (N_T=2000)	Frequency error ($N_T = 10,000$)
1	0.0232	0.0082
3	0.0370	−0.0032
3	0.0288	0.0013
4	0.0209	−0.0012
5	0.0045	−0.0004
6	0.0050	−0.0007

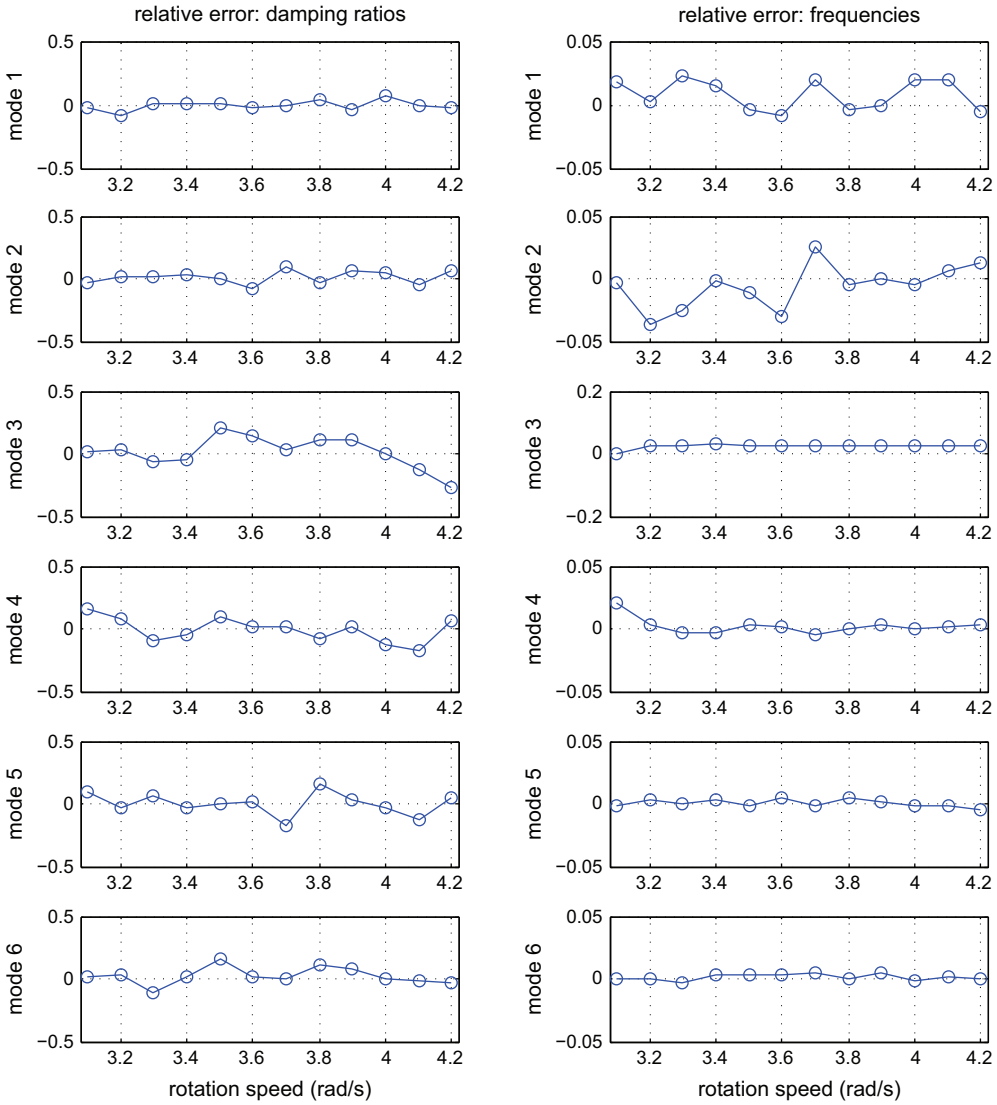

Fig. 3. Relative errors w.r.t. rotation speed Ω.

The classical SSI algorithm identifies some modes but is largely wrong for the first two modes. The new algorithm identifies all the modes and is more accurate for the last four modes thought it uses much less data samples than the classical algorithm. This identification goes of course more accurate when the sample length gets larger as shown in Table 3 where the relative errors of the identified frequencies using the new algorithms are computed for N_T=2000 and $N_T = 10,000$.

The new algorithm is also applied for simulation data set with varying rotation speed Ω from 3.1 rad/s to 4.2 rad/s by a step of 0.1 rad/s, and data were simulated over a number N_T=2000 of periods for each step of Ω. The relative errors of the new algorithm are plotted toward the rotation speed and reported in Fig. 3. The variation of the identified frequencies and

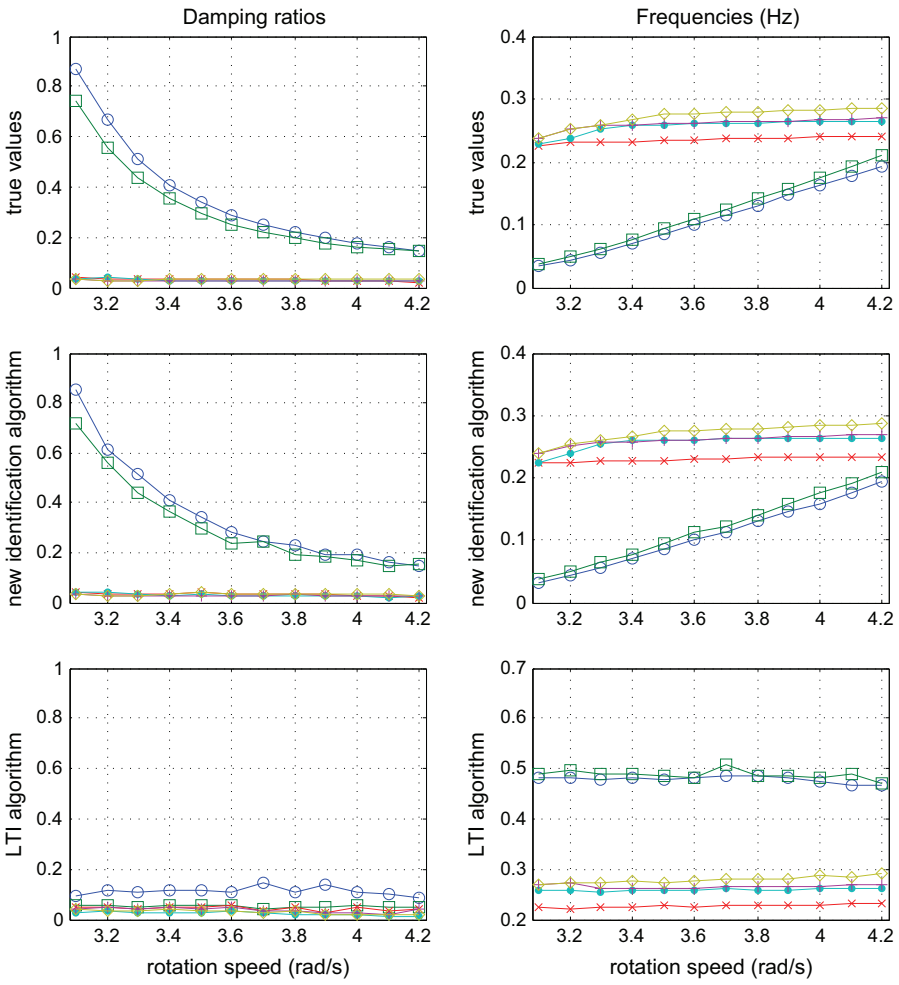

Fig. 4. Modes variation w.r.t. rotation speed Ω. On the left: the damping ratios. On the right: the frequencies. The top two figures are the true values. The bottom two figures: identification results by the classical SSI algorithm. And in the middle: identification results by the new SSI.

damping ratios using the new and the classical algorithms, as well as the variation of the true values, is given in Fig. 4. One can notice that the modes identified by the new algorithm track the true modes, whereas the classical algorithm gives modes with different variations.

Another feature to test is that these identified frequencies and damping ratios do not change over time as shown in Eq. (21), for a different choice of the index j (j being a parameter for Algorithm 1) (see Fig. 1). The variation of the estimated frequencies and damping ratios is plotted at $\Omega = 3.5$ rad/s, over a period (from the sample $j=q$ to $j = q+T_d$), and they are indeed constant as shown in Figs. 5 and 6.

It is also important to notice that the classical algorithm manages to identify correctly some of the modes (Table 2), because the considered rotation speed is close to the critical speed $\Omega = 4.4$ rad/s of the ground resonance where the fuselage (time-invariant part) and the rotor (time-periodic part) are coupled. When the rotation speed is far from 4.4 rad/s, this classical algorithm gives totally irrelevant results. Table 4 shows this for $\Omega = 2$ rad/s, for example. It shows the identified frequencies using the two algorithms as well as the true frequencies. The classical algorithm uses much more data samples N=200,000 than the new algorithm N_T=2000, however its identified modes are still highly biased.

4.4. Comparison with other approaches

As mentioned in the Introduction, works on the identification of LPTV systems remain limited. Under the assumption of isotropy, the identification could be handled with the so-called Coleman transformation or multi-blade transformation (MBC) [43], which allows to write the underlying system in the rotating frame, and then to obtain a time-invariant model. This approach has been recently suggested in [44] where the MBC transform is used as a pre-processing step to the classical SSI algorithm. The isotropy assumption must be not only internal but external, also: the rotor blades of the considered system have the same static structural properties, and the external loads are symmetric [37]. The latter symmetry is

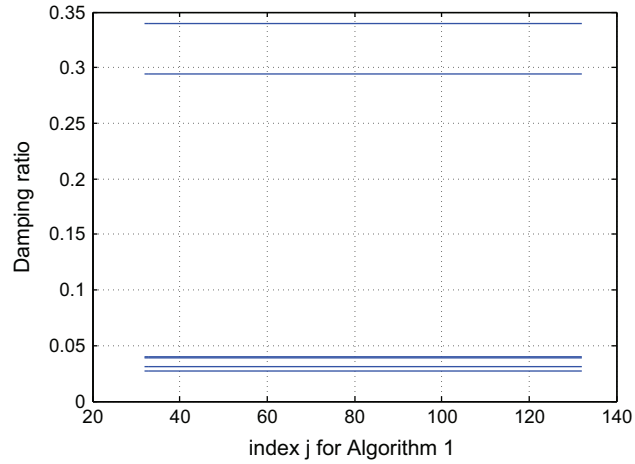

Fig. 5. Damping estimates for index j, over a period, for Algorithm 1 at $\Omega = 3.5$ rad/s.

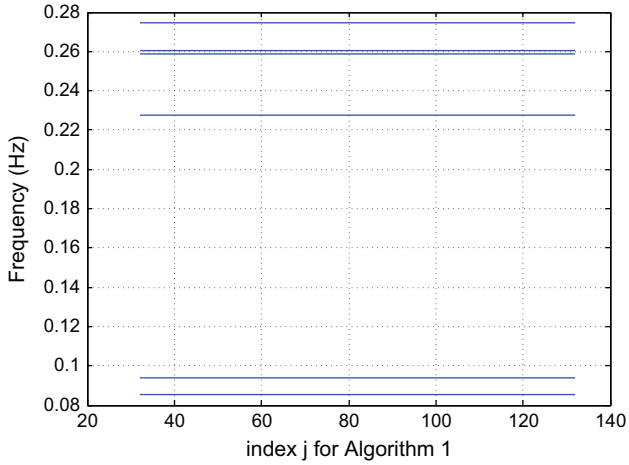

Fig. 6. Frequency estimates for index j, over a period, for Algorithm 1 at $\Omega = 3.5$ rad/s.

Table 4
Frequency estimates compared to true values for $\Omega = 2$ rad/s.

Mode	Classical SSI (Hz)	New SSI (Hz)	True values (Hz)
1	0.2171	0.0576	0.0586
2	0.2451	0.0732	0.0728
3	0.2451	0.0732	0.0728
4	0.2527	0.0995	0.0997
5	0.4791	0.1458	0.1481
6	0.4807	0.1559	0.1617

guaranteed when the system is operating in vacuum and is then quickly violated for real applications. In fact, the dynamic properties of the system (mainly the dynamic stiffnesses) may change drastically with the external loads such as aero-elastic and gravity loads as shown in [45,37]. In this case, the inherent periodic behavior cannot be completely suppressed and should be taken into account for the modal analysis [45,46]. This analysis is provided by the Floquet theory.

To the authors' knowledge, the work of Allen in [26] is the only work which deals with the output-only identification of the Floquet modes. The suggested approach uses a theory developed by Wereley in [29] regarding harmonic transfer functions (HTF), and the expression of the output spectrum in terms of the Floquet modes in order to estimate these latter

modes with the peak picking technique. As mentioned by Allen, the picking is based on a prior knowledge about the system and some spectra rays were neglected and were still uninterpreted.

The approach presented in the current paper does not require a prior knowledge of system dynamics and seems to give good estimates of the Floquet modes. At first sight, having fewer points for the new SSI algorithm ($N_T = N/T_d$) may appear as a potential drawback compared to the classical SSI which uses more data samples. This drawback is overcome by the fact that the new algorithm is not biased unlike the classical one as illustrated by the numerical application.

Besides, an algorithm is defined by its bias (consistency) and variance properties (efficiency). In this paper, it has been demonstrated that for one realization of the noise sequence, the algorithm provides estimated quantities close to the true ones. Considerations on the efficiency are pure assumptions and conjectures at this point. It has to be proved by a much heavier tool set. Efficiency of subspace methods for linear time-invariant approaches has been considered by the authors recently (see [47]). The extension of this study to the algorithm suggested herein is the scope of a future work.

5. Conclusion

The problem of identification for linear periodically time-varying is addressed. A new subspace-based algorithm is proposed. It has the aim to identify the so-called discrete-time monodromy matrix and its eigenvalues. This matrix is derived from the Floquet transformation which gives an equivalent description of periodic systems. Its eigenvalues, the Floquet multipliers, replace the classical eigenvalues in the classical modal analysis for linear time-invariant systems.

For this, a subspace matrix was built over lagged output data subsequences. Then, the matrix was extracted from a least squares minimization equation. The suggested algorithm is finally tested on data created from the simulation of a hinged blades helicopter spinning on the ground. Future works will focus on both the estimation of the uncertainties associated to the identified parameters and the validation with experimental data from helicopters and wind turbines.

Appendix A. Proof of Proposition 3.1

The elements of the Hankel matrix in (24) are products between lagged outputs y_{j+m} and y_{j-l}. These products write

$$\begin{aligned} y_{j+m}y_{j-l}^T = {} & \tilde{C}_{j+m}F^{m+l}z_{j-l}y_{j-l}^T \\ & + \tilde{C}_{j+m}F^{m+l-1}\tilde{v}_{j-l+1}y_{j-l}^T \\ & + \tilde{C}_{j+m}F^{m+l-2}\tilde{v}_{j-l+2}y_{j-l}^T \\ & + \cdots \\ & + \tilde{C}_{j+m}F\tilde{v}_{j+m-1}y_{j-l}^T \\ & + \tilde{C}_{j+m}\tilde{v}_{j+m}y_{j-l}^T \\ & + w_{j+m}y_{j-l}^T \end{aligned} \tag{A.1}$$

The observation matrix $\tilde{C}$ is periodic. Then $\tilde{C}_{j+iT_d} = \tilde{C}_j$, $\forall i > 0$. Now, let us compute the sum:

$$\begin{aligned} \sum_{i=0}^{N_T-1} y_{j+m+iT_d}y_{j-l+iT_d}^T = {} & \tilde{C}_{j+m}F^{m+l}\sum_{i=0}^{N_T-1} z_{j-l+iT_d}y_{j-l+iT_d}^T \\ & + \tilde{C}_{j+m}F^{m+l-1}\sum_{i=0}^{N_T-1} \tilde{v}_{j-l+1+iT_d}y_{j-l+iT_d}^T \\ & + \cdots \\ & + \tilde{C}_{j+m}F\sum_{i=0}^{N_T-1} \tilde{v}_{j+m-1+iT_d}y_{j-l+iT_d}^T \\ & + \tilde{C}_{j+m}\sum_{i=0}^{N_T-1} \tilde{v}_{j+m+iT_d}y_{j-l+iT_d}^T \\ & + \sum_{i=0}^{N_T-1} w_{j+m+iT_d}y_{j-l+iT_d}^T \end{aligned} \tag{A.2}$$

Dividing by N_T leads to:

- $\tilde{C}_{j+m}F^{m+l}(1/N_T)\sum_{i=0}^{N_T-1} z_{j-l+iT_d}y_{j-l+iT_d}^T$ converges to $\tilde{C}_{j+m}F^{m+l}G^{(j-l)}$ when N_T goes large, where $G^{(j-l)}$ is the correlation between the $(j-l)$−th time-invariant subsequences of the state vector and the output vector.
- $\tilde{C}_{j+m}F^{m+l-1}(1/N_T)\sum_{i=0}^{N_T-1} \tilde{v}_{j-l+1+iT_d}y_{j-l+iT_d}^T$ converges to 0 when N_T goes large, because w is a white noise which is uncorrelated of any time-invariant subsequence of the output, *idem* for $\tilde{C}_{j+m}F^{m+l-2}(1/N_T)\sum_{i=0}^{N_T-1} \tilde{v}_{j-l+2+iT_d}y_{j-l+iT_d}^T$, …, $\tilde{C}_{j+m}F(1/N_T)\sum_{i=0}^{N_T-1} \tilde{v}_{j+m-1+iT_d}y_{j-l+iT_d}^T$ and $\tilde{C}_{j+m}(1/N_T)\sum_{i=0}^{N_T-1} \tilde{v}_{j+m+iT_d}y_{j-l+iT_d}^T$.
- $(1/N_T)\sum_{i=0}^{N_T-1} w_{j+m+iT_d}y_{j-l+iT_d}^T$ converges to 0 too (unless when $m = l = 0$, which is not the case herein), for the same reason of uncorrelation.

Appendix B. Energies' expressions

B.1. Kinetic energy

According to the theorem of Koenig, the total kinetic energy of one blade is the sum of the kinetic energy of the circular translation, and that of the rotation about the center of mass of the blade:

$$T_{pk} = \tfrac{1}{2} m \dot{z}_k \dot{\bar{z}}_k + \tfrac{1}{2} I_z \dot{\phi}_k^2 \tag{B.1}$$

where m is the mass of the blade, Ω is the angular velocity of the main rotor, I_z is the moment of inertia of the k-th blade about its center of mass, $z = x + iy$ and $z_k = x_k + iy_k = z + (a + be^{i\phi_k})e^{i(\Omega t + \alpha k)}$ is the coordinate of the k-th blade, with $\alpha = 2\pi/(N_b - 1)$ and N_b is the number of blades. Then for small displacements ϕ_k, the kinetic energy of one blade writes

$$\begin{aligned} T_{pk} = {} & \tfrac{1}{2} m [\dot{z}\dot{\bar{z}} + \dot{\bar{z}} ib(\dot{\phi}_k + i\Omega\phi_k) e^{i(\Omega t + \alpha k)} + \dot{z}(-ib)(\dot{\phi}_k - i\Omega\phi_k) e^{-i(\Omega t + \alpha k)} \\ & + b^2 \dot{\phi}_k^2 - \Omega^2 ab\phi_k^2] + \tfrac{1}{2} I_z \dot{\phi}_k^2 \end{aligned} \tag{B.2}$$

Finally, the total kinetic energy of the helicopter writes

$$T = \frac{1}{2} M \dot{z}\dot{\bar{z}} + \sum_{k=0}^{N_b - 1} T_{pk} \tag{B.3}$$

B.2. Potential energy

The potential energy of the helicopter originates from the stiffnesses of the fuselage in the two directions x and y, modeled in Fig. 2 by two springs, and the stiffnesses of the N_b blades. The total potential energy is then the sum of the separate energies:

$$U = \frac{1}{2} K_z z\bar{z} + \frac{1}{2} \sum_{k=0}^{N_b - 1} K_{\phi_k} \phi_k^2 \tag{B.4}$$

B.3. Dissipation function

Dampers are added to the model considered in [41]. Its incorporation in the structure provides more stability to it, by absorbing the oscillation of the landing gear and reducing the lead lagging modes on the rotor. This stabilizing effect is discussed in [48,49] who considered dampers on the rotor. The dampers are assumed to be linear. Nonlinear dampers can be replaced by equivalent linear viscous damping using a standard linearization technique [50]. Similar to the potential energy, the dissipation function can be written as

$$F = \frac{1}{2} C_z \dot{z}\dot{\bar{z}} + \frac{1}{2} \sum_{k=0}^{N_b - 1} C_{\phi_k} \dot{\phi}_k^2 \tag{B.5}$$

Appendix C. System matrices

The system matrices write

$$\mathcal{M} = \begin{bmatrix} (M + N_b m) & 0 & -mb.\sin_0 & \cdots & \cdots & -mb.(\sin)_{N_b - 1} \\ 0 & (M + N_b m) & mb.\cos_0 & \cdots & \cdots & mb.(\cos)_{N_b - 1} \\ -mb.\sin_0 & mb.\cos_0 & (mb^2 + I_z) & 0 & \cdots & 0 \\ \vdots & \vdots & \vdots & \ddots & & \\ -mb.(\sin)_{N_b - 1} & mb.(\cos)_{N_b - 1} & 0 & 0 & \cdots & (mb^2 + I_z) \end{bmatrix}$$

$$\mathcal{C} = \begin{bmatrix} C_x & 0 & -2\,mb\Omega.\cos_0 & \cdots & -2\,mb\Omega.(\cos)_{N_b - 1} \\ & C_y & -2\,mb\Omega.\sin_0 & \cdots & -2\,mb\Omega.(\sin)_{N_b - 1} \\ & & C_{\phi_0} & & \\ & & & \ddots & \\ & & & & C_{\phi_{N_b - 1}} \end{bmatrix}$$

$$\mathcal{K} = \begin{bmatrix} K_x & 0 & mb\Omega^2.sin_0 & \cdots & mb\Omega^2.(sin)_{N_b-1} \\ & K_y & -mb\Omega^2.cos_0 & \cdots & -mb\Omega^2.(cos)_{N_b-1} \\ & & K_{\phi_0}+m\Omega^2 ab & & \\ & & & \ddots & \\ & & & & K_{\phi_{N_b-1}}+m\Omega^2 ab \end{bmatrix}$$

where $sin_k = \sin(\Omega t+\alpha k)$, $cos_k = \cos(\Omega t+\alpha k)$ and $\alpha = 2\pi/(N_b-1)$.

References

[1] C. Desoer, Slowly varying discrete system $xi+1 = aixi$, Electronics Letters 6 (11) (1970) 339–340.
[2] M. Freedman, G. Zames, Logarithmic variation criteria for the stability of systems with time-varying gains, SIAM Journal on Control 6 (3) (1968) 487–507.
[3] L. Ljung, System Identification: Theory for the User, vol. 7632, Prentice Hall, New Jersey, 1987.
[4] A.H. Sayed, Fundamentals of Adaptive Filtering, John Wiley & Sons, 2003.
[5] Y. Li, H.-l. Wei, S.A. Billings, Identification of time-varying systems using multi-wavelet basis functions, IEEE Transactions on Control Systems Technology 19 (3) (2011) 656–663.
[6] R. Zou, H. Wang, K.H. Chon, A robust time-varying identification algorithm using basis functions, Annals of Biomedical Engineering 31 (7) (2003) 840–853.
[7] Z. Qizhi, L. Li, Identification of time-varying system based on fourier series, in: WRI Global Congress on Intelligent Systems, GCIS'09, vol. 2, IEEE, 2009, pp. 44–47.
[8] M. Niedzwiecki, T. Klaput, Fast recursive basis function estimators for identification of time-varying processes, IEEE Transactions on Signal Processing 50 (8) (2002) 1925–1934.
[9] M. Verhaegen, X. Yu, A class of subspace model identification algorithms to identify periodically and arbitrarily time-varying systems, Automatica 31 (2) (1995) 201–216.
[10] K. Liu, Identification of linear time-varying systems, Journal of Sound and Vibration 206 (4) (1997) 487–505.
[11] K. Liu, Extension of modal analysis to linear time-varying systems, Journal of Sound and Vibration 226 (1) (1999) 149–167.
[12] K. Liu, L. Deng, Experimental verification of an algorithm for identification of linear time-varying systems, Journal of Sound and Vibration 279 (3) (2005) 1170–1180.
[13] P. Van Overschee, B. De Moor, Subspace Identification for Linear Systems: Theory, Implementation, Applications, Kluwer Academic Publishers, 1996.
[14] M. Majji, J.-N. Juang, J.L. Junkins, Time-varying eigensystem realization algorithm, Journal of Guidance, Control, and Dynamics 33 (1) (2010) 13–28.
[15] K. Josic, R. Rosenbaum, Unstable solutions of nonautonomous linear differential equations, SIAM Review 50 (3) (2008) 570–584.
[16] É. Mathieu, Mémoire sur le mouvement vibratoire d'une membrane de forme elliptique, Journal de mathématiques pures et appliquées 2e série, tome 13 (1868) 137–203.
[17] G. Floquet, Sur les équations différentielles linéaires à coefficients périodiques, Annales Scientifiques de l'École Normale Supérieure 12 (1883) 47–88.
[18] J.A. Richards, Analysis of Periodically Time-varying Systems, Springer-Verlag, Berlin, 1983.
[19] P. Montagnier, C.C. Paige, R.J. Spiteri, Real Floquet factors of linear time-periodic systems, Systems & Control Letters 50 (4) (2003) 251–262.
[20] S. Bittanti, P. Colaneri, Periodic Systems: Filtering and Control, Springer, London, 2009.
[21] L. Sanches, G. Michon, A. Berlioz, D. Alazard, Instability zones for isotropic and anisotropic multibladed rotor configurations, Mechanism and Machine Theory 46 (8) (2011) 1054–1065.
[22] L. Sanches, G. Michon, A. Berlioz, D. Alazard, Parametrically excited helicopter ground resonance dynamics with high blade asymmetries, Journal of Sound and Vibration 331 (16) (2012) 3897–3913.
[23] C.C. Ross, Differential Equations: An Introduction with Mathematica®, Springer, 2004.
[24] S.C. Sinha, E. Butcher, Symbolic computation of fundamental solution matrices for linear time-periodic dynamical systems, Journal of Sound and Vibration 206 (1) (1997) 61–85.
[25] E.A. Butcher, H. Ma, E. Bueler, V. Averina, Z. Szabo, Stability of linear time-periodic delay-differential equations via Chebyshev polynomials, International Journal for Numerical Methods in Engineering 59 (7) (2004) 895–922.
[26] M.S. Allen, M.W. Sracic, S. Chauhan, M.H. Hansen, Output-only modal analysis of linear time-periodic systems with application to wind turbine simulation data, Mechanical Systems and Signal Processing 25 (4) (2011) 1174–1191.
[27] M. Allen, J.H. Ginsberg, Floquet modal analysis to detect cracks in a rotating shaft on anisotropic supports, in: 24th International Modal Analysis Conference (IMAC XXIV), 2006.
[28] M. Allen, Floquet experimental modal analysis for system identification of linear time-periodic systems, in: ASME 2007 International Design Engineering Technical Conferences & Computers and Information in Engineering Conference, 2007.
[29] N.M. Wereley, S.R. Hall, Frequency response of linear time periodic systems, in: Proceedings of the 29th IEEE Conference on Decision and Control, IEEE, 1990, pp. 3650–3655.
[30] A. Benveniste, J.-J. Fuchs, Single sample modal identification of a nonstationary stochastic process, IEEE Transactions on Automatic Control 30 (1) (1985) 66–74.
[31] T. Soderstrom, P. Stoica, System Identification, Prentice Hall International Series in Systems and Control Engineering, 1989.
[32] B. Peeters, G. De Roeck, Reference-based stochastic subspace identification for output-only modal analysis, Mechanical Systems and Signal Processing 13 (6) (1999) 855–878.
[33] M. Basseville, A. Benveniste, M. Goursat, L. Hermans, L. Mevel, et al., Output-only subspace-based structural identification: from theory to industrial testing practice, ASME Journal of Dynamic Systems, Measurement, and Control 123 (4) (2001) 668–676. (Special issue on Identification of mechanical systems).
[34] M. Goursat, L. Mevel, Algorithms for covariance subspace identification: a choice of effective implementations, in: Proceedings of the IMAC XXVII, Florida, USA, 2009.
[35] M. Basseville, M. Abdelghani, A. Benveniste, Subspace-based fault detection algorithms for vibration monitoring, Automatica 36 (1) (2000) 101–109.
[36] J.J. DaCunha, J.M. Davis, A unified Floquet theory for discrete, continuous, and hybrid periodic linear systems, Journal of Differential Equations 251 (11) (2011) 2987–3027.
[37] P. Skjoldan, Aeroelastic Modal Dynamics of Wind Turbines Including Anisotropic Effects, Ph.D. Thesis, Technical University of Denmark, 2011.
[38] R. Meyer, C. Burrus, A unified analysis of multirate and periodically time-varying digital filters, IEEE Transactions on Circuits and Systems 22 (3) (1975) 162–168.
[39] A. Jhinaoui, L. Mevel, J. Morlier, Subspace identification for linear periodically time-varying systems, in: Proceedings of the 16th IFAC Symposium on System Identification (SYSID), 2012, pp. 1282–1287.
[40] A. Jhinaoui, L. Mevel, J. Morlier, Extension of subspace identification to lptv systems: application to helicopters, in: Topics in Modal Analysis I, vol. 5, Springer, 2012, pp. 425–433.

[41] L. Sanches, G. Michon, A. Berlioz, D. Alazard, Instability zones identification in multiblade rotor dynamics, in: 11th Pan-American Congress of Applied Mechanics, 2010.
[42] J. Wang, I. Chopra, Dynamics of helicopters in ground resonance with and without blade dissimilarities, in: AIAA Dynamics Specialists Conference, Dallas, TX, 1992, pp. 273–291.
[43] G. Bir, Multi-blade coordinate transformation and its applications to wind turbine analysis, in: ASME Wind Energy Symposium, 2008.
[44] D. Tcherniak, S. Chauhan, M. Rossetti, I. Font, J. Basurko, O. Salgado, Output-only modal analysis on operating wind turbines: application to simulated data, in: European Wind Energy Conference, 2010.
[45] K. Stol, H. Moll, G. Bir, H. Namik, A comparison of multi-blade coordinate transformation and direct periodic techniques for wind turbine control design, in: 47th AIAA Aerospace Sciences Meeting, 2009.
[46] L. Sanches, Helicopter Ground Resonance: Dynamical Modeling, Parametric Robustness Analysis and Experimental Validation, Ph.D. Thesis, ISAE, 2011.
[47] M. Döhler, X.-B. Lam, L. Mevel, Uncertainty quantification for modal parameters from stochastic subspace identification on multi-setup measurements, Mechanical Systems and Signal Processing 36 (2013) 562–581.
[48] D.L. Kunz, Influence of elastomeric damper modeling on the dynamic response of helicopter rotors, AIAA Journal 35 (1997) 349–354.
[49] D.L. Kunz, Nonlinear analysis of helicopter ground resonance, Nonlinear Analysis: Real World Applications 3 (3) (2002) 383–395.
[50] L. Pang, G.M. Kamath, N.M. Wereley, Analysis and testing of a linear stroke magnetorheological damper, in: Proceedings of the 39th AIAA/ASME/ASCE/AHS/ASC Structures, Structural Dynamics, and Materials Conference and Exhibit and AIAA/ASME/AHS Adaptive Structures Forum, 1998, pp. 2841–2856.